



Synergistic effect of gallic acid lipid nanoparticles to improve the physicochemical property and cellular uptake against MDA MB 231 Cancer cell line: Apoptosis, signaling pathway and cytotoxicity

Sandhiya .V^{1*}, Priyanka Sinha², T.Sathish Kumar³, R. Siva kumar⁴, Swetha B⁵, Deepika A⁶, Sona Jain P⁷, Theresa Evangilin P⁸

^{1,2,3,4,5,6,7,8}Department of pharmaceutics, C.L.Baid metha college of pharmacy, Thoraipakkam, Chennai-97

*Corresponding author: Sandhiya.V, Assistant professor C.L.Baid metha college of pharmacy, Email: Sandhiyavaithi@gmail.com

Submitted: 14 January 2023; Accepted: 27 February 2023; Published: 20 March 2023

ABSTRACT

Introduction: Gallic acid (GA), a phenolic molecule that occurs naturally, has been shown to have anti-tumor properties for a number of cancer types. The effect of GA on breast tumor cells MDA-MB-231 Triple Negative was examine in the current study.

Methods: Techniques were utilised for cell cycle analysis, GSH concentration, Annexin V assay, light and fluorescence microscopy, restriction of cell growth (MTT assay), preparation, characterisation, and measurement of the mitochondrial membrane potential.

Results: It was shown that the produced GANP significantly reduced the ability of MDAMB-231 cells to multiply. Moreover, this might result in glutathione depletion, an increase in ROS levels, and cytotoxic activity in MDA-MB-231 cells. Analysis using flow cytometry revealed so as to the GANP enhanced the inhabitants of sub-G1 cells. Also, the Annexin V/PI test and fluorescence labelling both established so as to the addition of GA dramatically increased the amount of apoptotic cells. Therefore, research of the oxidative damage-related sickness revealed that the amalgamation of GA greatly decrease oxidative damage in healthy cells while increasing glutathione levels and lowering lipid peroxidase levels in MDA-MB-231 cells

Conclusion: These consequences propose that GA as GANP may have potential as a chemopreventive treatment for triple negative breast cancer.

Keywords: Apoptosis, triple negative breast cancer

INTRODUCTION

Breast cancer is the most frequent reason of cancer-related death worldwide, with more than a million novel cases being identified every year. According to research, the distribution of cancer rates among immigrant populations is similar to the distribution in the nation of residence. The incidence of breast cancer varies by region.

This shows that non-genetic lifestyle decisions, including nutrition, may have an impact on the development of cancer.

According to research on both humans and animals, the oestrogen receptor (ER) is involved in bone metabolism, reproduction, neuroendocrine and cardiovascular system modulation, as well as sexual

behaviour and development in both sexes. Tamoxifen, the most popular endocrine treatment medicine and the most commonly prescribed anti-estrogen, is linked to a more aggressive tumour phenotype and decreased susceptibility to ER gene expression reduction. This significantly contributes to the spread of breast cancer. Tamoxifen, a medication that is sold over the counter, binds to the oestrogen receptor, stops it from working, and stops the growth of breast cells. Myeloid Cell Leukemia-1 is a member of the Bcl-2 gene family and one of the most effective antiapoptotic agents for regulating ER appearance and cancer cell survival [1]. The survival of hematogenous and solid tumour cells is impacted by the oncogene Mcl-1. Mcl-1 down-regulation is necessary but insufficient to cause apoptosis to begin..

several chemotherapeutic moiety endorse the synthesis of pro-apoptotic molecules including P53, which controls cellular stress through mitochondrial and death receptor-mediated apoptotic pathways. appearance of exacting molecular markers, such as P21, influences whether cancer cells will ultimately become malignant cells. The progression of the cell cycle is regulated by P21WAF1/CIP, which also functions as a common inhibitor of cyclin-dependent kinases. Tumorigenesis and other oncogenic mutations result from P21 deficiency. P21 can affect the way other positive cell cycle regulators work, and since cancer cells make more P21 than normal cells do, it is more challenging to "stop" cell growth at the G1 checkpoint. The ability of P21 to improve cell cycle inhibition may depend on its power to mediate P53-dependent gene suppression, given that P21 is both necessary and enough for P53-dependent repression of the genes driving cell cycle advancement. On the other hand, in response to particular cellular stresses, P21 may cause cell death through P53-dependent and P53-independent pathways. The main goal of efficient anticancer medications is to kill cancer cells by activating signalling pathways that lead to apoptosis [2].

Fruits, vegetables, coffee, and phenolic acids, including gallic acid (3, 4, 5-trihydroxybenzoic acid), may have anti-cancer, anti-inflammatory,

antibacterial, immunoregulatory, and antioxidant properties. Two proposed mechanisms for their anticancer actions comprise enhancing P53 and P21 gene expression and decreasing CDK2 gene appearance, which may cause a G0/G1 cell cycle arrest [3]. Although recent research has linked these substances to the development of some tumours, the fundamental mechanisms are yet unknown.

The aspire of this learn was to examine the property of gallic acid and gallic acid-loaded nanoparticles on the triple negative breast cancer cell line and their impacts on the anti-breast cancer effects. Also, the impact of the chemical on cell cycle analysis, morphological cell changes, and enzymatic analysis of cells was looked into. We concentrated on the intrinsic apoptotic signalling system, which is a prominent apoptosis route, and the relationship between these genes and prospective treatment possibilities [4]. We evaluated these chemicals' interactions with cancer cells using receptor binding activity to understand the principles underlying how GA-induced regulation of breast carcinogenesis works. In order to detect morphological and proliferative alterations[5].

MATERIALS AND METHODS

Materials

The Merck Corporation sold GA to GA (Germany). The subsequent compounds were purchased from Sigma-chemical Co. in St. Louis, Missouri: 2,7-dichlorodihydrofluorescein diacetate (DCFDA), rhodamin123, 5-dithiobis (2-nitrobenzoic acid), 3-(4,5-dimethylthiazol-2-yl) MTT, acridine orange, ethidium bromide, sulfanilamide, N-1-naphthylethylenediaminedihydrochloride (NED), and RNase A are examples of tetrazolium compounds.

Cell Signaling Corporation provided the antibodies (UK). From Gibco Co., we acquired RPMI 1640 medium, Trypsin/EDTA, and Fetal Bovine Serum (FBS) (Grand Island, USA). Amersham Bioscience provided the ECL kit and Polyvinylidenedifluoride (PVDF) membrane (Arlington Heights, USA). Roche Life Sciences'

Annexin V-Fluos staining kit was obtained (Penzberg, Germany).

Methods

Preparation of standard curve

The stock solution was diluted to 10 mcg/ml. Using the same solvent, the secondary stock solution was now diluted to produce solutions with concentrations of 2, 4, 6, 8, and 10 (mcg/ml). A standard plot was placed next to the regression line after the solution had been analyzed with a UV/VIS spectrophotometer at 264 nm [6].

Pre-formulation Studies

Before being transformed into a dosage form, a pharmaceutical substance must be chemically and physically defined. Using the knowledge gained from preformulation studies, researchers can devise a plan for mixing a pharmacological agent with pharmaceutical excipients to produce a dosage form. The drug's physicochemical profile is We used descriptive language to notice and record organoleptic characteristics, such as colour and scent.

Determination of melting point and solubility

To decide the substance's melt point, a little quantity of the drug was put in a capillary tube that was closed at one end. It is additionally linked to the thermometer that is positioned in the middle of a heating bath in order to track the temperatures at which melting begins and stops and to gradually heat the bath [7]. The equilibrium solubility method was used to calculate the solubility. Separate doses of gallic acid were injected into screw-capped beaker vials that held 5ml of the solvent [8]. The vials were automatically shaken on a shaker for 24 hours. The combination was centrifuged at 6000 rpm for 20 minutes after 24 hours.

Pre-formulation studies

The parameters of pre-formulation studies was carried out as per standard procedures given in IP

Procedure

The solid lipid nanoparticles were produced by the nanoprecipitation procedure. A precise amount of soy lecithin (10 mg) and gallic acid (20 mg) be dissolve in ethanol and then agitated with TPP at the proper rpm for 10 minutes. The solution was then dropped into a 10 ml solution of 1% v/v aqueous acetic acid, poloxmer, and chitosan while being stirred [9]. To evaporate the ethanol, the resultant dispersion was stirred at 800 rpm at space temperature for a whole night. After being collected, the nanoparticles were centrifuged at 13,500 rpm for an hour, three times in distilled water, and then lyophilized to produce a dry powder of nanoparticles.

Drug Encapsulation Efficiency (EE) and Loading Capacity (LC)

Using a centrifugal filter tube and the filtering method, the EE (%) and LC values of GA-loaded SLNs be planned. The unloaded GA must be dissolved, and then isolated from the dispersed SLNs in order to compute the EE correctly. After the GA particles were diluted with ethanol to dissolve them, a sample of the preparation which included SLNs and likely unloaded GA was obtained. The dissolve GA was then alienated from the SLNs by centrifuging it for 10 minutes at 5000 rpm [10]. The GA in the obvious solution at the base of the tube was found using UV-visible with a maximum wavelength of 264 nm.

FTIR

FTIR examines the rotation and vibration of molecules using a particular infrared light wavelength. Infrared spectroscopy is based on the discovery that electromagnetic radiation in the infrared area vibrates at a frequency that matches that of the link atoms, producing a series of vibrational motions. This vibrational motion is brought on when infrared rays enter a molecule. 100 mg of KBr discs and 10 mg of each sample were used in the spectroscopy. Then, 30 mg of the mixture was crushed at 15 tonnes for 10 seconds to produce clean discs for IR spectra [11].

DSC and XRD

DSC was used to examine the following substances: gallic acid, chitosan, GA-Chi, SLN, and SLN-PF68. The Central Instrumentation Laboratory (CIL) at the Vels Institute of Science and Technology used a DSC-3 series device. Samples were dried for 48 hours at 55°C without the use of a cryoprotectant after being submerged in liquid nitrogen for 15 minutes to freeze dry SLNs. Nitrogen gas flowing at a rate of 20 ml/min and a scan rate of 20 °C/min were both used to evaluate the samples (5 mg). 40 to 350 °C was the temperature range used for the analysis. An X-ray Diffractometer Smart lab model produced the X-ray diffraction patterns for the samples. It was a scan with an angle range of 5° to 50°.

In vitro dissolution study

The dialysis bag diffusion technique was used to analyze the results of the in vitro drug release testing of the GA-NPs formulations. The following step involved using a beaker with 20 millilitres of pH 4.8 phosphate buffer, 0.1% SDS (v/v), and 2.5% tween 80 (v/v), as well as a dialysis bag with two millilitres of drug-loaded nanoparticles. To keep the assembly's temperature at 37 °C during the experiment, the beaker was set over a magnetic stirrer [13]. The experiment's target speed was set at 100 revolutions per minute (rpm). Each time, a new 100 L of dialysis buffer was introduced in place of the 100 L sample that had been taken out. The samples were then assessed using a 264 nm UV-visible spectrophotometer..

Kinetic study

Kinetic study-KorsmeyerPeppas model

A simple semi-empirical model developed by Korsmeyer exponentially connects the release of medication to the passage of time (t).

$$Kk_{tn} = Q_t/Q$$

This release behaviour study can be used by the formulator to compare results [14]. The release exponent can be obtained from the slope of the graph between the left side of the equation's

logarithmic versions and log t, and the constant can be found from the intercept (Kk).

Nanoparticle size determination

A laser particle size analyzer was used to determine the mean size distribution, mean nanoparticle size, and polydispersity index (Shimadzu SALD-2300). After being diluted in double-distilled water, each batch of nanoparticles was filtered separately (0.22 m). Three average size measurements were taken for each set. Plots of the results were made according to the number and size of the nanoparticles.

SEM

The sample is sprinkled on double-sided carbon tape and placed on a brass stub. The surface is coated with a thin layer of palladium (about 30 µm) in an auto fine coater [15]. Then, it is placed in the sample chamber of a scanning electron microscope and the morphology of the complex is observed.

Zeta potential study

Surface zeta potentials will be measured using the laser zeta meter. Liquid samples of the nanoparticles (5ml) have to be diluted with double distilled water (50 ml) using NaCl as suspending electrolyte solution (2 x10⁻² m NaCl) [16,17]. The pH has to be adjusted to the required value. The samples are to be shaken for 30 minutes. After shaking, the equilibrium pH has to be recorded and the zeta potential of the particles should be measured. The results are shown in Fig 9

Particle size

The analysis has to be carried out at a scattering angle of 90° at a temperature of 25°C using nanoparticles dispersed in deionized distilled water (2 mg of sample was dissolved in 5ml of deionized water and then sonication has to be done in a sonicator. Particle size distributions of the nanoparticles are to be reported as a polydispersity index.

TEM

The structure of SLN and c-SLN was examined using transmission electron microscopy (TEM). Using the JEOL-2100F at a 100 kV accelerating voltage, the samples were evaluated. A drop of the SLN dispersion was used to create a thin liquid layer on a copper grid that had been coated with carbon. After five minutes, the additional sample was collected using filter paper [18]. The sample was then naturally dried at room temperature after being negatively stained with 2% phosphotungstic acid to increase contrast..

In-vitro cell line study

It is possible to show that the manufactured GANPs had a negative impact on the viability of human cancer cells using the cellular toxicity assay 3-(4, 5-dimethylthiazol-2-yl)-2,5-diphenyl tetrazolium bromide (MTT). Individual cells were seeded into 96-well plates at a cell density of 5 10⁵ cells per well. Cells were starved for an hour at 37°C after being washed twice with 100 L of media devoid of serum for 24 hours. Following a fast, cells were exposed to increasing doses of the test medication (20 L) for 48 hours at 37 °C in a humidified 5% CO₂ environment. The addition of 40 L of MTT solution per well was done after the initial 4 hours of medium incubation. On an ELISA microplate reader, the purple-blue formazan dye was measured spectrophotometrically at 570 nm (ELx808 Absorbance Reader). Once the experiment was carried out three times, the average number of viable cells was determined. The percentage of viable cells and dilution were displayed on a graph [19, 20]. The information was presented as a percentage of relative viability for vehicle control.

AO double staining

The addition of 40 L of MTT solution per well was done after the initial 4 hours of medium incubation. On an ELISA microplate reader, the purple-blue formazan dye was measured spectrophotometrically at 570 nm (ELx808 Absorbance Reader). Once the experiment was carried out three times, the average number of viable cells was determined. The percentage of

viable cells and dilution were displayed on a graph [19, 20]. The information was presented as a percentage of relative viability for vehicle control.

Cell cycle analysis

To investigate the apoptotic effect of PF68 loaded GANPs 1x10⁵ cells were seeded in 1.98 mL of growth medium and incubated for 24 hours at 37°C with 5% CO₂. After incubation, 20 µL GANPs were added to the concentration of drugs ranging from 50, 100, 300, and 500 g/mL for MCF-7 cell lines. Then, these treated cells were continually fostered in the medium at 37°C with 5% CO₂ for 72 hours [21,22]. Untreated cells were used as a control group. After incubation, the cells were transferred to a falcon tube and centrifuged at 800 rpm for 5 minutes. When centrifugation was completed, the pellet was dissolved in 5 mL of PBS and centrifuged another time. Then resuspended in 200 µL of buffer added to 2 L of Annexin V-FITC and PI. The stained cells were incubated for 15 minutes at room temperature. Finally, the mixture was determined by a flow cytometer.

Measurement of glutathione levels

The 5'-thio-2-nitrobenzoic acid (TNB), which is visible at 412 nm and may be used to quantify glutathione, is created by first oxidising GSH with the sulfhydryl reagent 5,5'-dithio-bis(2nitrobenzoic acid) (DTNB). At the beginning, we produced the cell lysate and measured the glutathione level using the DTNB reagent and a spectrophotometer calibrated to 412 nm.

Measurement of mitochondrial membrane potential

Cells were cultured in 35 mm culture dishes with Nunc cover glass that was covered in collagen. Cells were grown for four hours in new medium containing 30 g mL⁻¹ of GANPF68 nanoparticles after a 24-hour incubation period. The nuclei and mitochondria were stained with DAPI (1 g mL) and JC-1 for 30 minutes, respectively, in fresh medium in place of the nanoparticle-containing

solution (1 g mL). After three PBS rinses, the cells were fixed for 15 minutes using 4% paraformaldehyde in PBS. The cover glasses were imaged using the Olympus FluoView FV1000 confocal microscope following anti-fade mounting solution mounting on a glass slide (Vector Laboratories).

Antioxidant Activity

With a slight modification to the previously published DPPH scavenging test method, the formulations' antioxidative activity was assessed. Several amounts of ascorbic acid (a positive control) were made in an ethanol solution, ranging from 5 to 50 g/mL. A positive control was utilised, acid ascorbicum. To test different formulation concentrations, we made a 2 mL batch of 0.1 mM DPPH-ethanol solution. A UV-Vis spectrophotometer (UV-2600, Shimadzu, Tokyo, Japan) set to a wavelength of 520 nm is used to measure the absorbance after fully vortexing the combined solutions and 30 minutes of room temperature incubation in the dark [23, 24]. The DPPH scavenging percentage was calculated using the following equation:

$$\text{DPPH scavenging percentage (\%)} = \left[\frac{\text{Absorbance test}}{\text{Absorbance control}} \right] 100\%$$

Stability study

After being freeze-dried and combined with phosphate buffered saline, pH 7.4, the GA-NPs

were maintained at 4 °C for three months while being protected from light. At intervals of 0 days, 1 month, and 3 months, NPs' particle size, PDI, and zeta potential were assessed [25].

RESULT AND DISCUSSION

Pre-formulation studies: Pre-formulation parameter results show that the drug and polymer have good flow characteristics and can be used to produce nanoparticles.

Drug's physicochemical description:

All nine formulas created a uniformly smooth surface texture that was dry, elastic, and yellow, according to the results of an organoleptic investigation. Alcohol and ethanol made the chemical soluble, while water did not.

Melting point determination: According to research, the melting point of gallic acid is 274°C.

Study on solubility determination

According to the solubility analysis, glycerin is not soluble in water but is soluble in alcohol. Moreover, it is easily dissolved by ethanol. Solubility increases with particle size due to the larger surface area in contact with the solvent. Gallic acid-containing medicine dissolves considerably better in ethanol than in water. Table 1 displays the results.

TABLE 1: Gallic acid solubility study

Reagents	samples	Solubilized gallic acid (mg/ml)
Aqueous medium	Gallic acid	0.02 ± 0.003
acetonitril	Gallic acid	3.32 ± 0.08
Ethanol	Gallic acid	4.21 ± 0.01

TABLE 2: entrapment efficiently and drug loading of gallic acid nanoparticles

Formulation code	EE (%)	PDI	SIZE (nm)	LC (mg/g)
F1	72.2±1.8	0.54±0.01	218.6±2.1	32.4±0.4
F2	74.3±0.1	0.45±0.03	248.1±0.1	30.6±0.2
F3	70.9±9.1	0.56±0.06	232.5±9.1	33.9±0.1

F4	71.1±0.3	0.63±0.02	208.4±0.2	40.1±0.4
F5	82.4±2.2	0.46±0.01	195.6±1.2	42.6±0.1
F6	80.9±2.2	0.34±0.02	198.9±2.1	43.8±0.2
F7	80.1±1.1	0.52±0.02	183.4±2.1	47.4±0.1
F8	84.8±0.3	0.38±0.01	147±.4±0.9	48.9±0.2

FTIR

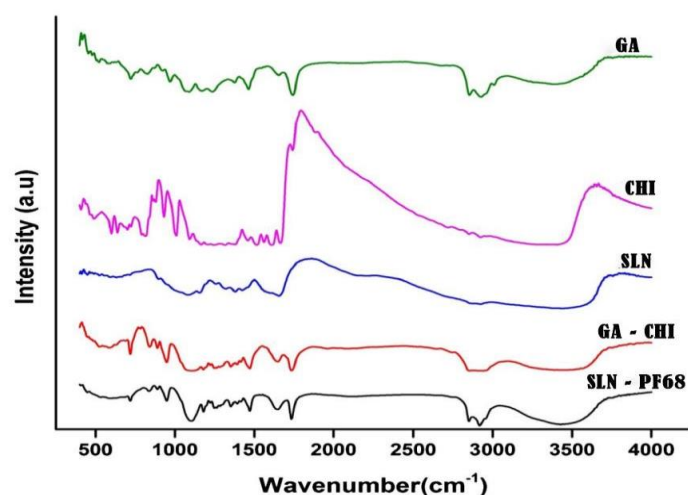


FIG 1: FTIR spectrum of GA(Gallic acid), CHI (Chitosan). SLN(Gallic acid loaded solid lipid nanoparticles). GA-CHI (Gallic acid and Chitosan) and SLN-PF68 (Gallic acid loaded lipid nanoparticles with surfactants)

Gallic acid nanoparticles underwent FTIR analysis. The molecular link between gallic acid and the chitosannanocarrier is verified using FTIR. Figure 1 [26] shows the results of the FTIR examination of the nanoparticles. The aromatic hydroxyl (-OH) group between 3200 and 3500 cm^{-1} , the carbonyl (-C=O) group at 1702 cm^{-1} , and the aromatic carbon between 1500 and 1600 cm^{-1} were all clearly visible in the FTIR spectrum of gallic acid. Figure 2 shows the infrared spectra of the chitosan polymer, which are The large absorption peak visible in this image in the (3273-3446) cm^{-1} region is caused by the stretching vibration of the interfering bonds (O-H) and (N-H) [27].].

The absorption beam visible in (2881) cm^{-1} is the result of the (C-H) finger's stretching and bending vibration. Conversely, it is thought that the (1656) cm^{-1} peak is brought on by the (N-H) bond's stretching vibration. The cyclotide bond stretching vibration (C-O-C) is visible as an apparent peak in the polymer FTIR spectrum of the chitosannanoparticle at (1155) cm^{-1} , however the alcohol groups' (C-O) bond vibration is perceptible as an apparent peak at (1022 cm^{-1}). A large hydroxyl (-OH) stretching, wide amine group (-N-H) band, and broad N-H bands at 3200 cm^{-1} are also visible. Moreover, the relationship between gallic acid and the chitosannanocarrier has been shown by a very wide absorption band at 3000-3700 cm^{-1} in the FTIR spectra of gallic acid nanoparticles (fig. 1).

XRD

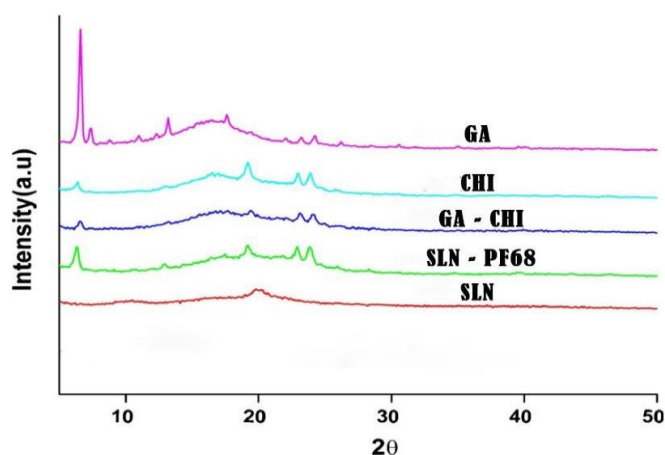


FIG 2: XRD diffractogram of GA(Gallic acid), CHI (Chitosan). SLN(Gallic acid loaded solid lipid nanoparticles). GA-CHI (Gallic acid and Chitosan) and SLN-PF68 (Gallic acid loaded lipid nanoparticles with surfactants)

When X-ray diffraction technology is used, the chemical composition, crystalline structure, and small size of the produced compounds are all thoroughly described. The X-ray diffraction of the polymer and GA-loaded chitosan nanoparticles is shown in Figure 2 [28]. The peaks at 16.43°, 19.2°, and 23.96°, respectively, correspond to the crystallographic planes for gallic acid, poloxamer F68, and amorphous chitosan. The polymer is amorphous, as indicated by the large peak at 2 of roughly 200. No other

peaks that would suggest the produced chitosan is of high purity also don't show up. The CS nanoparticles' XRD pattern, Both of the biomolecules' peaks, which had peaks at angles higher than the diffraction angle, vanished, showing that they had been absorbed into the nanoparticles in an amorphous condition. The formulations' extraordinarily high crystalline biomolecule encapsulation efficacy in comparison to untrapped molecules is more evidence for this conclusion [29].

DSC

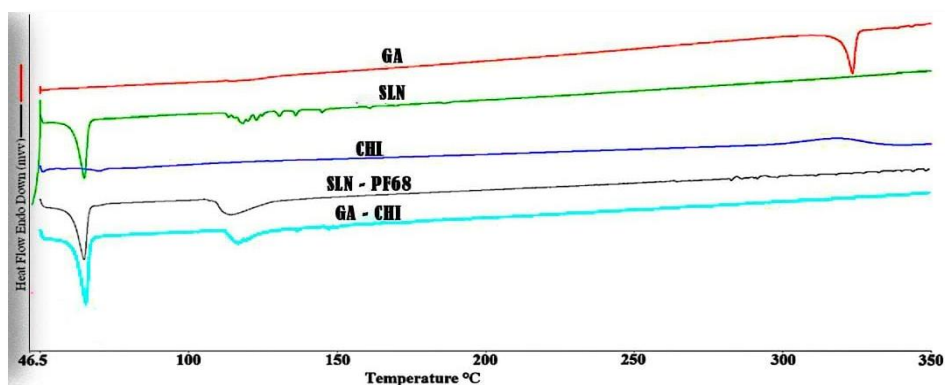


FIG 3: DSC thermogram of GA(Gallic acid), CHI (Chitosan). SLN(Gallic acid loaded solid lipid nanoparticles). GA-CHI (Gallic acid and Chitosan) and SLN-PF68 (Gallic acid loaded lipid nanoparticles with surfactants)

Gallic acid displayed distinct endothermic peaks at 129.94 °C and 259.68 °C, which were in agreement with their melting temperatures. The peak of gallic acid at 91.73 °C may have been caused by moisture evaporation [30]. On the Poloxamer 307 thermogram, the endothermic peak, which occurred at 58.92 °C, could be seen (Fig. 3). However, the thermogram of chitosan showed a noticeably bigger endothermic peak at roughly 84.37 °C (Fig. 3). The thermogram of the

physical combination only shows the superimposition of individual components and gives no indication of interaction (Fig. 3). As evidenced by the absence of the unique main peak of biomolecules near the end of the crystalline DSC thermogram of CS nanoparticles, gallic acid has completely enclosed the nanoparticles, changing their state from crystalline to molecularly dispersed amorphous (Fig. 3).

In-vitro dissolution study

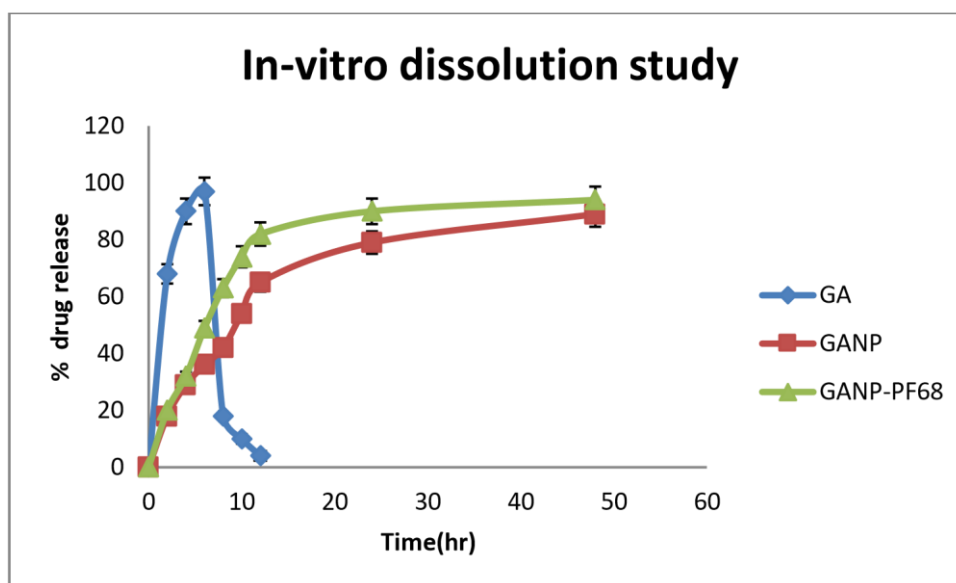


FIG 4 : in-vitro dissolution profile of GANP-PF68

Chi nanoparticles that were GA-loaded underwent in vitro dialysis in the tumour cells' acidic pH environment. In general, the investigations were conducted at pH 4.8. the 96 percent of the loaded GA was released after 48 hours of incubation in PBS, according to our findings. The drug is progressively released over 48 hours, based on the release profile of nanoparticles loaded with GANP-PF68 in an acidic environment (Figure 4). The drug molecules, which were only loosely linked to the surface of the chitosan nanoparticles, dissociated to create the effect. Furthermore, it is evident how their close proximity to nanoparticle surfaces affects the first rapid release of protein. The second characteristic of the release profile is the slow, roughly constant release of drug

molecules from nanoparticles. After 48 hours, it seems that the drug is breaking down more quickly than it is releasing.

Kinetic study

The plots revealed that the zero order equation best explained the drug release data and had the highest linearity ($r^2=0.975$), followed by Higuchi's equation ($r^2= 0.941$). The optimum option for drug release was zero order kinetics, hence it is presumed that the rate of drug release is concentration independent. The mechanism of drug release was found using the Korsmeyer-Peppas equation, which demonstrated strong linearity ($r^2= 0.959$). The diffusion exponent "n," which ranged from 0.5 to 1.0, indicating a non-

fickian diffusion process. Also, it demonstrates that a variety of processes, such as diffusion and

dissolution, were used to control the drug's release. [31].

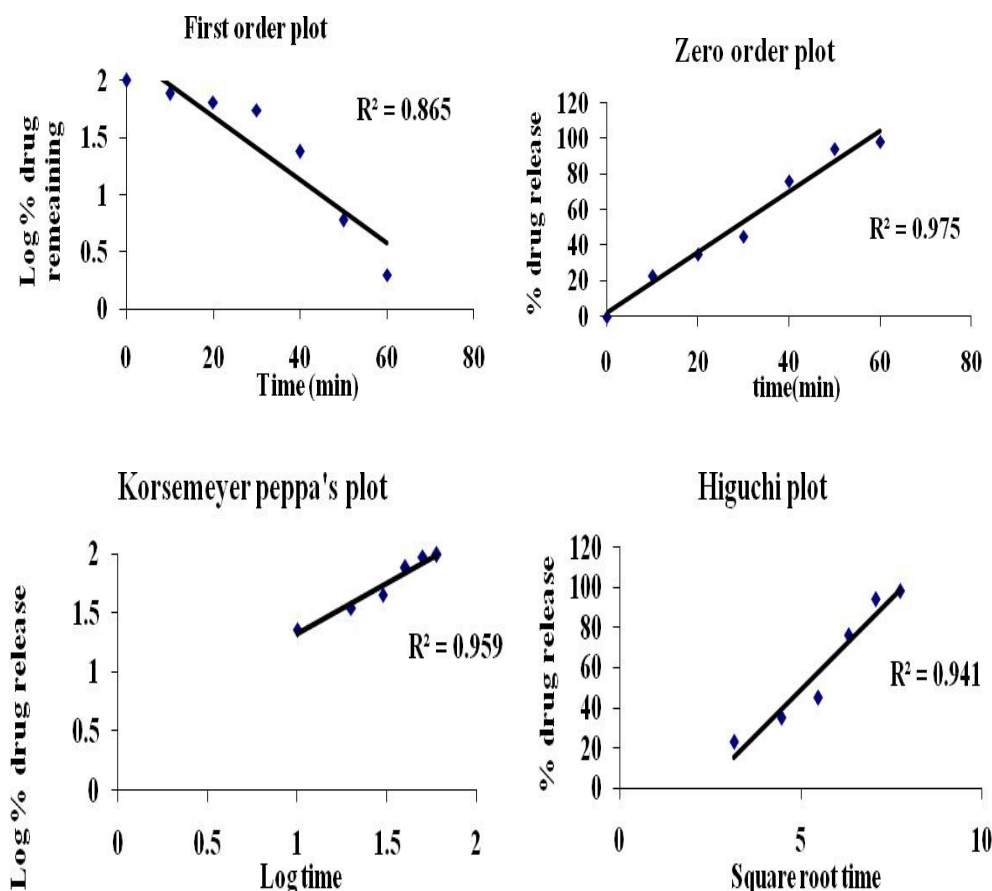


FIG 5: Kinetic release modeling of optimized formulation

Antioxidant activity

Using the DPPH assay, the capacity of free and nano-encapsulated gallic acid to scavenge free radicals in vitro was assessed. While evaluating the antioxidant activity of various compounds, the stability of the organic free radical DPPH is taken into consideration. Trolox was a suitable choice for a control because it degrades in water. Due to the presence of GANPs nanoparticles, the DPPH in this test transformed from a dark violet to a light or colourless solution. GANPs had a

DPPH scavenging activity of 85.6% for the amounts of 200 g/mL, respectively, but free gallic acid had a scavenging activity of only 25.4%, 46.6%, and 62.3% for the same concentrations (p 0.05). In light of this, gallic acid's Even after being nanoencapsulated in gum arabic nanoparticles, the entire functioning was retained. At comparable concentrations, trolox demonstrated a significant scavenging activity of 94.6% against DPPH [32].

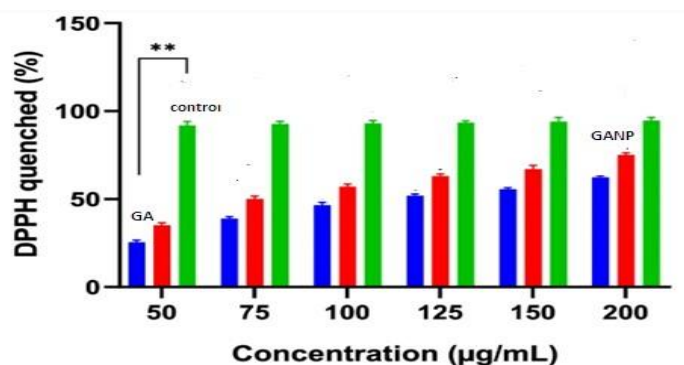


FIG 6: DPPH scavenging activity of GA and GANPs

Zeta potential

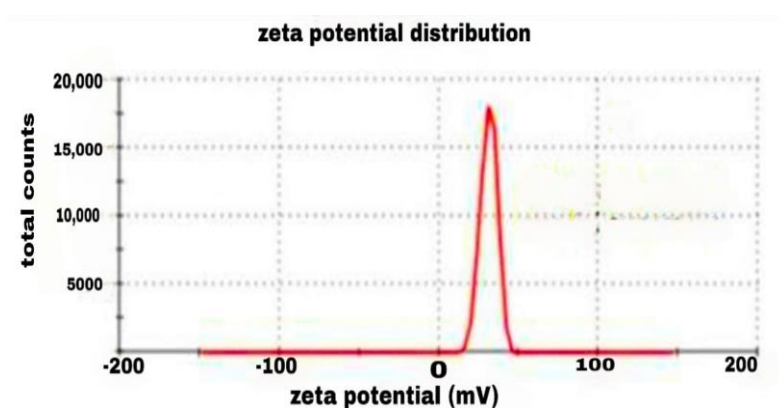


FIG 7: Zeta potential measurement of optimized formulation

The strength with which particles are brought together or maintained apart is measured by the zeta potential. Accurate measurement is crucial for electrostatic dispersion management since it reveals the mechanism. Several sectors, including brewing, ceramics, pharmaceuticals,

medicine, mineral processing, and water treatment, depend on zeta potential evaluation. Zeta potential was 43.4 mV, or mV. Due to its cationic makeup, chitosan was discovered to have a higher zeta potential of 42.8 mV. [33].

SEM and TEM

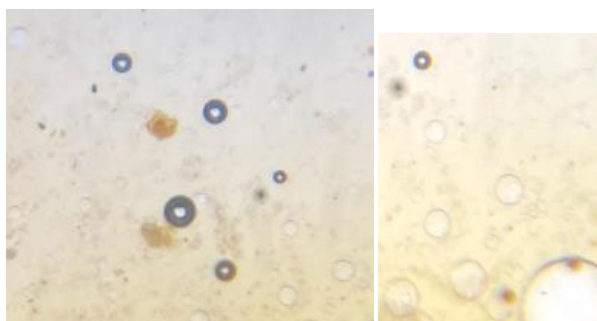


FIG 7 A): Optical microscopic images of prepared nanoparticles

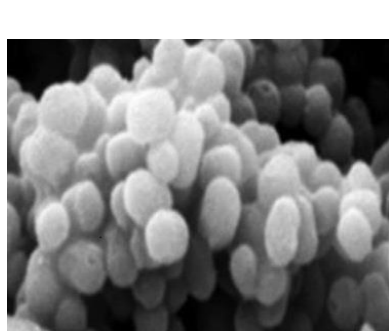


FIG 7 B): SEM of optimized formulation

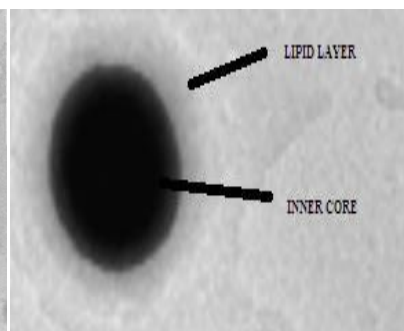
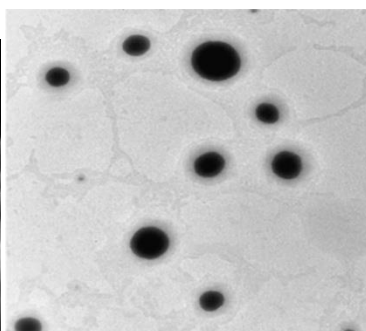


FIG 8: TEM of optimized formulations

The new formulation's SEM photography, as seen in fig. 9, displays a spherical shape with a smooth, rounded surface. The TEM image suggests that the particle is crosslinked and thick, and that the high density of the polymer would enable the formulation to have a controlled release. The surface morphology of the optimized formulation was also validated by TEM. The production of vesicles was amply demonstrated by the TEM study of the nanoparticle, which displayed a black, spherical nanoparticle against a light backdrop. The generated nanoparticle was appropriately identified as having a bilayer lipid membrane, an usually spherical morphology, and a range of nanometric sizes, as is evident from the results. Moreover, nanoparticles showed no signs

of fusion or aggregation, and pictures showed that they were smooth, spherical, and free of drug crystals. The outcome was displayed in fig 8.

In-Vitro Cell Line Study

To determine the vitality of the MDA-MB-468 cells, an MTT experiment was conducted. Figure depicts the effects of GA treatment after 24 and 48 hours on MDA-MB-468 cells. Figure 9 demonstrates how the GA treatment considerably raised the cell inhibitory rate when compared to the control group. These findings demonstrated that GA significantly reduced the viability of triple-negative breast cancer cells [34].

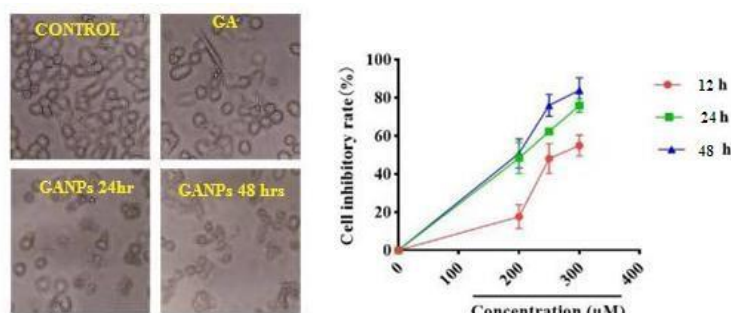


FIG 9: in-vitro cell line study of optimized formulation

Using an inverted microscope, the morphology of the triple negative breast cancer cells changed after treatment with various GA doses for up to 48 hours (0, 200, 250, and 300 M). Figure 9 depicts the control group's cells, which were in great condition, were still attached to the wall,

had a distinct cell contour, and had a high cell density. The GA treatment groups' cells, on the other hand, shrank, had fractured nuclei, had lower cell densities, and were in an apoptotic state [35].

AO/EB fluorescent staining study

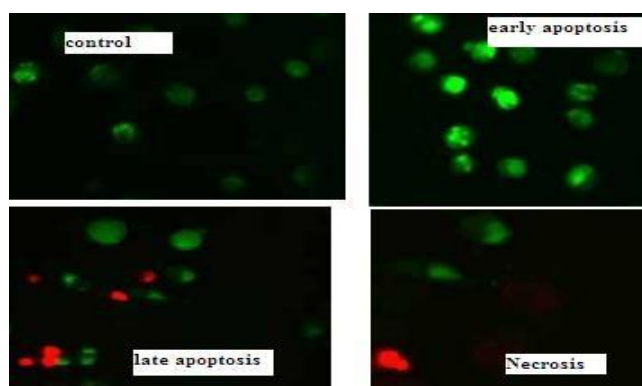
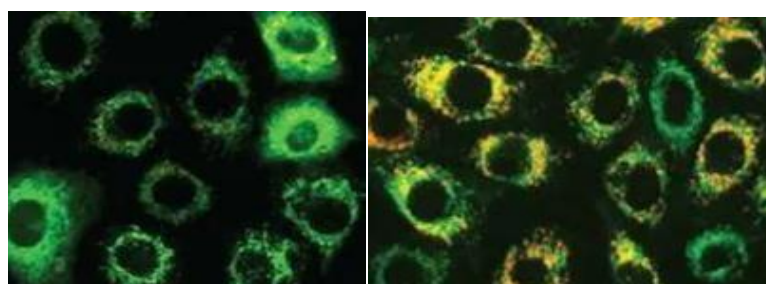


FIG 10: Fluorescent staining study of optimized formulation

(AO/EB) fluorescence labelling, which may be viewed with a fluorescent microscope, can be used to spot apoptotic changes in cell membranes [36]. The negative control group had no apoptotic symptoms (Figure 10). Yellow green AO nuclear staining with crescent or granular morphology identified cells in the experimental group that were in the early stages of apoptosis. Staining was unevenly distributed inside the cells [25].

Larger doses and longer treatment times led to an increase in early-stage apoptotic cell numbers. Asymmetrically distributed late-stage apoptotic cells with strongly orange nuclear EB staining were also discernible. (See Figure 10.) Necrotic cells made up a greater percentage of the population, and their edges fluoresced unevenly in an orange-red colour. The cells appeared to be dividing (figure 10).

Mitochondrial membrane potential study



A)Control B)GANP-PF68

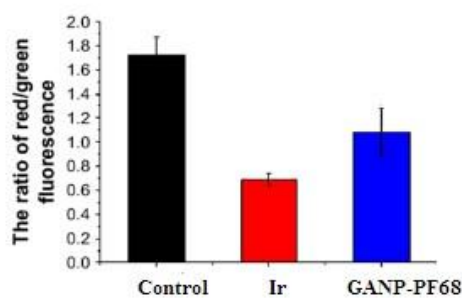


FIG 11: Mitochondrial membrane potential study of GA and GANPs

As seen in Figure 11, the mitochondria were labelled red after coming into contact with the cells, and the GANP-PF68 released green fluorescence [32,33]. Red and green fluorescence combining indicates that GANP-PF68 may penetrate the mitochondria [37, 38]. JC-1 was used as a fluorescent probe to examine how GANP-PF68 affected the changes in MMP. When MMP is high, JC-1 aggregates and emits red fluorescence; when MMP is low, JC-1 emits green fluorescence. [34] Figure 11 shows that JC-1 fluoresces red in the control [39]. When 3 M of GANP-PF68 (a positive control) is incubated with JC-1 for 24 hours, the fluorescence is mainly

green with very little red. The fact that the fluorescence changed from red to green shows that GANP-PF68 can destroy MMP. The red/green fluorescence ratio was computed with MateXpress6 to more precisely compare how GANP-PF68 affected the alterations in MMP. The red/green fluorescence ratio for the control was 1.72 to 0.16, as shown in Figure 4B. The red/green fluorescence ratios were 0.69/0.06 and 1.08/0.21 following a 24-hour GANP-PF68 treatment, respectively. The findings demonstrate that measuring glutathione and MDA levels

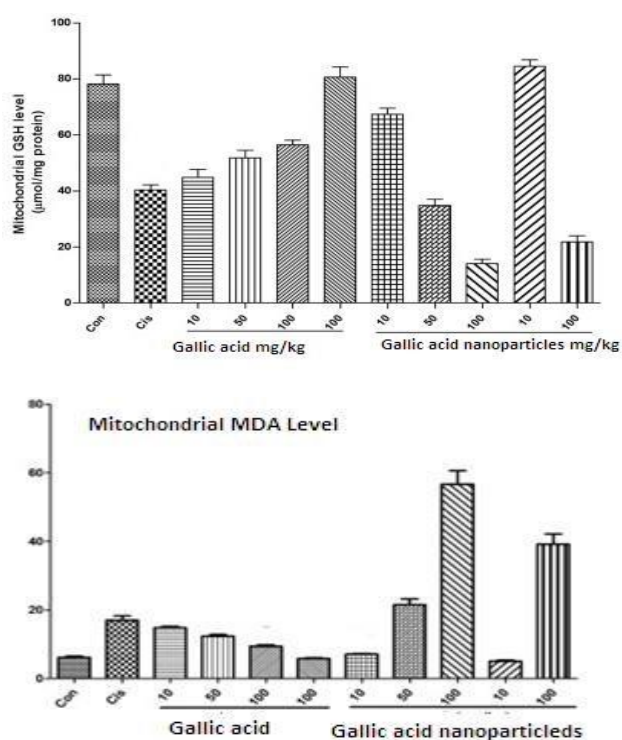


FIG 12: Measurement of GPX and MDA levels of GA and GANPs

The level of mitochondrial GSH in the cisplatin group significantly decreased when compared to the control group (P 0.001). Gallic acid (50 mg/kg), nano-gallic acid (10 mg/kg), and gallic acid (100 mg/kg) groups received significantly higher levels of renal mitochondrial GSH than the cisplatin group (P 0.01). The renal mitochondrial MDA level significantly increased in the cisplatin group compared to the control group (P 0.001). Gallic acid (100 mg/kg) and

nano-gallic acid (10 mg/kg) treatment groups had renal mitochondrial MDA levels that were significantly lower than those of the cisplatin group (P 0.01). Renal mitochondrial GSH was considerably lower in the group treated with gallic acid 50 mg/kg than in the group treated with nano-gallic acid (P 0.01). The renal mitochondrial GSH was higher in the 10 mg/kg nano-gallic acid treatment group compared to the 100 mg/kg gallic acid treatment group, despite

the difference not being statistically significant [42]. Between the control group and the nanogallic acid 10 and 100 mg/kg alone groups, there were no differences in the levels of renal mitochondrial GSH and MDA. However, when nanogallic acid 100 mg/kg was administered alone and in the treatment group, the renal

mitochondrial GSH level was dramatically decreased and the renal mitochondrial MDA level was elevated in comparison to the control group. These results illustrated the risk associated with the dosage of nanoparticles. Assessment study of nuclear morphology

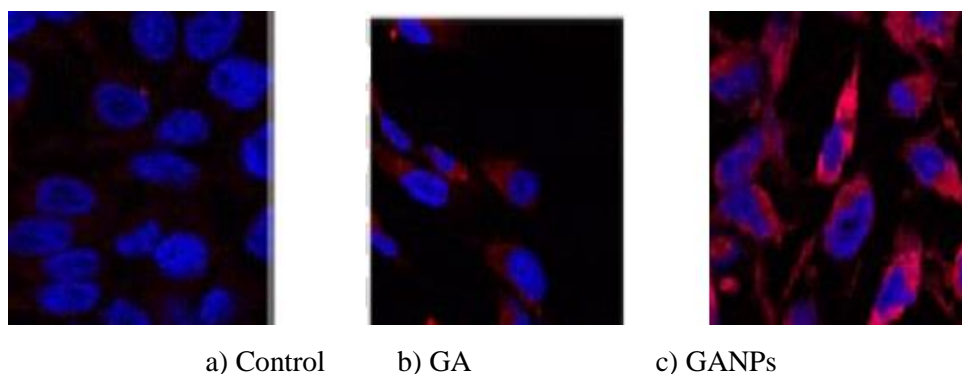


FIG 13: Morphological assessment study of GA and GANPs

It is possible to swiftly identify between viable, apoptotic, and necrotic cells using nucleus morphology. Fluorescence microscopy was used to examine how DAPI labelling affected apoptosis (Figure 13). Pictures of the stained cells with DAPI reveal that, as compared to GA, GA-loaded SLNs (Figure 13 c) significantly speed up chromatin breakdown or nucleus condensation (Figure 13C) [43]. The study's positive and negative controls were cells that had not been treated (Figure 13 A) and cells that had been treated with 5% DMSO (Figure 13).

Particle Size Distribution

Dynamic light scattering was employed with the ZetasizerNano S90 to calculate the polydispersity index (PDI) and particle size distribution of the SLN dispersion [44]. After being properly diluted with distilled water, the dispersion was seen using a disposable cuvette at 25°C (18.2 M cm¹). After each measurement was finished, the mean size and PDI were calculated using at least three sets of 15 runs.

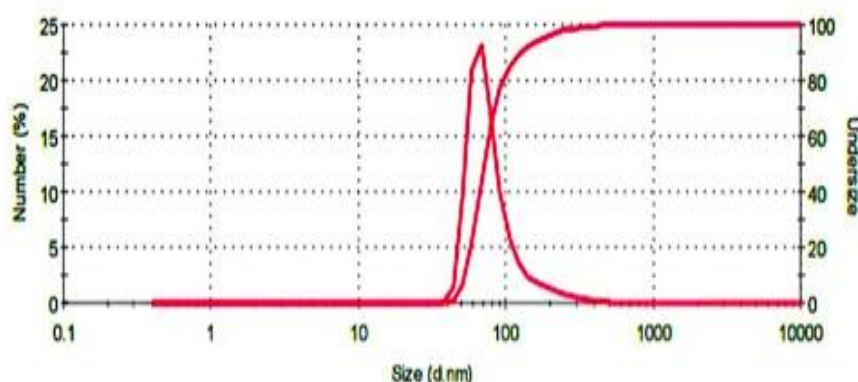


FIG 14: Determination of particle size of GANPs

Stability studies

According to ICH recommendations, investigations on the enhanced formulations' short-term stability were done. As well as 25°C/60%RH and 4°C, the storage conditions employed for stability studies were 37°C and 75%RH. Following in-vitro

release, a sample of GANPs was examined for its physical characteristics, drug content, and release properties at 0 and 6 months. The NCs were examined, and the results are displayed in Table No. 3. The findings showed that none of the characteristics showed a significant difference.

TABLE 3: stability study of prepared nanoparticles

Code	Conditions	Time	Assay(%)	In-vitro release
GANP-PF68	25±2°C/ 60±5% RH	6	99.4	96.3
	37±2°C/75±5% RH	6	98.6	95.9
	4±2°C	6	98.4	95.4

CONCLUSION

The results of the present investigation imply that the apoptotic properties of PF-68 nanoparticles coated with the naturally occurring phenolic component GA may have been enhanced synergistically. It was discovered that GSH and MDA depletion followed by mitochondrial dysfunction are the main causes of apoptosis induction by creating PF-68 embedded nanoparticles, which can form pores, inhibit the efflux mechanism of cancer cells, and possibly be able to stimulate apoptosis in TNBCs, which rarely respond to chemotherapeutic agents. This demonstrates that NDDS therapy may be transformed into an effective, all-encompassing cancer treatment.

Contributions

SV designed the study, PS monitored the work and others performed the work

Corresponding author

Sandhiya.V

Ethical declaration

Not applicable

Consent for publication

All the authors are approved for publication

ACKNOWLEDGEMENT

We grateful to thank our college, Dr.MGR medical university and management

CONFLICT OF INTEREST

The authors declare that they have no conflict of interest

Funding

Not applicable

Author information

Sandhiya and priyanka

Faculty of pharmacy, department of pharmaceuticals, MGR university, Chennai, india

REFERENCES

1. Łukasiewicz, S., Czezelewski, M., Forma, A., Baj, J., Sitarz, R., & Stanislawek, A. (2021). Breast Cancer-Epidemiology, Risk Factors, Classification, Prognostic Markers, and Current Treatment Strategies-An Updated Review. *Cancers*, 13(17), 4287. <https://doi.org/10.3390/cancers13174287>
2. Ginsburg, O., Bray, F., Coleman, M. P., Vanderpuye, V., Eniu, A., Kotha, S. R., Sarker, M., Huong, T. T., Allemani, C., Dvaladze, A., Gralow, J., Yeates, K., Taylor, C., Oomman, N., Krishnan, S., Sullivan, R., Kombe, D., Blas, M. M., Parham, G., Kassami, N., ... Conteh, L.

- (2017). The global burden of women's cancers: a grand challenge in global health. *Lancet* (London, England), 389(10071), 847–860. [https://doi.org/10.1016/S0140-6736\(16\)31392-7](https://doi.org/10.1016/S0140-6736(16)31392-7)
3. Kahkeshani, N., Farzaei, F., Fotouhi, M., Alavi, S. S., Bahramsoltani, R., Naseri, R., Momtaz, S., Abbasabadi, Z., Rahimi, R., Farzaei, M. H., & Bishayee, A. (2019). Pharmacological effects of gallic acid in health and diseases: A mechanistic review. *Iranian journal of basic medical sciences*, 22(3), 225–237. <https://doi.org/10.22038/ijbms.2019.32806.7897>
 4. Rezaei-Seresht, H., Cheshomi, H., Falanji, F., Movahedi-Motlagh, F., Hashemian, M., & Mireskandari, E. (2019). Cytotoxic activity of caffeic acid and gallic acid against MCF-7 human breast cancer cells: An in silico and in vitro study. *Avicenna journal of phytomedicine*, 9(6), 574–586. <https://doi.org/10.22038/AJP.2019.13475>
 5. Brewster, A. M., Chavez-MacGregor, M., & Brown, P. (2014). Epidemiology, biology, and treatment of triple-negative breast cancer in women of African ancestry. *The Lancet. Oncology*, 15(13), e625–e634. [https://doi.org/10.1016/S1470-2045\(14\)70364-X](https://doi.org/10.1016/S1470-2045(14)70364-X)
 6. Shirazi, O. U., Khattak, M. M. A. K., & Shukri, N. A. M. (2014). Determination of total phenolic, flavonoid content and free radical scavenging activities of common herbs and spices. *Journal of Pharmacognosy and Phytochemistry*, 3(3), 104–108. https://www.phytojournal.com/vol3Issue3/Issue_sep_2014/29.1.pdf
 7. Gan, J. E., & Chin, C. Y. (2021). Formulation and characterisation of alginate hydrocolloid film dressing loaded with gallic acid for potential chronic wound healing. *F1000Research*, 10, 451. <https://doi.org/10.12688/f1000research.52528.1>
 8. Kaparekar, P. S., Pathmanapan, S., & Anandasadagopan, S. K. (2020). Polymeric scaffold of Gallic acid loaded chitosan nanoparticles infused with collagen-fibrin for wound dressing application. *International journal of biological macromolecules*, 165(Pt A), 930–947. <https://doi.org/10.1016/j.ijbiomac.2020.09.212>
 9. Ullah, K. H., Rasheed, F., Naz, I., Ul Haq, N., Fatima, H., Kanwal, N., & Ur-Rehman, T. (2022). Chitosan Nanoparticles Loaded Poloxamer 407 Gel for Transungual Delivery of Terbinafine HCl. *Pharmaceutics*, 14(11), 2353. <https://www.mdpi.com/1999-4923/14/11/2353/pdf>
 10. Mahboob, T., Nawaz, M., de Lourdes Pereira, M. et al. PLGA nanoparticles loaded with Gallic acid- a constituent of *Leea indica* against *Acanthamoeba triangularis*. *Sci Rep* 10, 8954 (2020). <https://doi.org/10.1038/s41598-020-65728-0>
 11. Singh, B., & Dhiman, A. (2015). Designing bio-mimetic moxifloxacin loaded hydrogel wound dressing to improve antioxidant and pharmacology properties. *Rsc Advances*, 5(55), 44666–44678. <https://pubs.rsc.org/en/content/getauthorversionpdf/C5RA06857F>
 12. Kamalakaran, A.S. Molecular Adducts of Isoniazid: Crystal Structure, Electronic Properties, and Hirshfeld Surface Analysis. *J Struct Chem* 59, 1518–1533 (2018). <https://doi.org/10.1134/S002247661807003X>
 13. Erdagi, S. I., & Yildiz, U. (2019). Diosgenin-conjugated PCL–MPEG polymeric nanoparticles for the co-delivery of anticancer drugs: Design, optimization, in vitro drug release and evaluation of anticancer activity. *New Journal of Chemistry*, 43(17), 6622–6635. <https://pubs.rsc.org/en/content/articlelanding/2019/nj/c9nj00659a>
 14. Wu, I. Y., Bala, S., Škalko-Basnet, N., & Di Cagno, M. P. (2019). Interpreting non-linear drug diffusion data: Utilizing Korsmeyer-Peppas model to study drug release from liposomes. *European Journal of Pharmaceutical Sciences*, 138, 105026. <https://www.sciencedirect.com/science/article/pii/S0928098719302908>
 15. Salehchah, M., Alboghobeish, S., Dehghani, M.A. et al. Multi-walled carbon nanotubes induce oxidative stress, apoptosis, and dysfunction in isolated rat heart mitochondria: protective effect of naringin. *Environ Sci Pollut Res* 27, 13447–13456 (2020). <https://doi.org/10.1007/s11356-020-07943-w>
 16. Pudake, R. N., Chauhan, N., & Kole, C. (Eds.). (2019). *Nanoscience for sustainable agriculture* (Vol. 711). Cham: Springer International Publishing. <https://link.springer.com/book/10.1007/978-3-319-97852-9>
 17. Chithrani, B. D., Ghazani, A. A., & Chan, W. C. (2006). Determining the size and shape dependence of gold nanoparticle uptake into mammalian cells. *Nano letters*, 6(4), 662–668. <https://doi.org/10.1021/nl052396o>
 18. Zhu, R., & Lu, S. (2010). A high-resolution TEM investigation of nanoparticles in soils. In *Molecular Environmental Soil Science at the Interfaces in the Earth's Critical Zone* (pp. 282–284). Springer Berlin Heidelberg. https://link.springer.com/chapter/10.1007/978-3-642-05297-2_81
 19. Askar, M. A., El-Nashar, H. A., Al-Azzawi, M. A., Rahman, S. S. A., & Elshawi, O. E. (2022). Synergistic Effect of Quercetin Magnetite Nanoparticles and Targeted Radiotherapy in Treatment of Breast Cancer. *Breast cancer : basic*

- and clinical research, 16, 11782234221086728. <https://doi.org/10.1177/11782234221086728>
20. Otoyá-Martínez, N., Leite, L. G., Harakava, R., Touray, M., Hazir, S., Chacon-Orozco, J., & Bueno, C. J. (2023). Disease caused by *Neofusicoccum parvum* in pruning wounds of grapevine shoots and its control by *Trichoderma* spp. and *Xenorhabdus szentirmaii*. *Fungal biology*, 127(1-2), 865–871. <https://doi.org/10.1016/j.funbio.2022.12.002>
 21. Zhang, K., Shen, Q., Fang, Y., Sun, Y., Ding, J., & Chen, Y. (2019). AZD9291 inactivates the PRC2 complex to mediate tumor growth inhibition. *Acta Pharmacologica Sinica*, 40, 1587–1595. <https://www.semanticscholar.org/paper/AZD9291-inactivates-the-PRC2-complex-to-mediate-Zhang-Shen/0a7b79d71dd5b9686ac8bb8197d89f6431398b8b>
 22. Dehghani, N., Tafvizi, F., & Jafari, P. (2021). Cell cycle arrest and anti-cancer potential of probiotic *Lactobacillus rhamnosus* against HT-29 cancer cells. *BioImpacts*: BI, 11(4), 245. <https://bi.tbzmed.ac.ir/Article/bi-22097>
 23. Konopko A, Kusio J, Litwinienko G. Antioxidant Activity of Metal Nanoparticles Coated with Tocopherol-Like Residues—The Importance of Studies in Homo- and Heterogeneous Systems. *Antioxidants*. 2020; 9(1):5. <https://doi.org/10.3390/antiox9010005>
 24. Rahman, M.M., Islam, M.B., Biswas, M. et al. In vitro antioxidant and free radical scavenging activity of different parts of *Tabebuia pallida* growing in Bangladesh. *BMC Res Notes* 8, 621 (2015). <https://doi.org/10.1186/s13104-015-1618-6>
 25. Wu Y-Z, Tsai Y-Y, Chang L-S, Chen Y-J. Evaluation of Gallic Acid-Coated Gold Nanoparticles as an Anti-Aging Ingredient. *Pharmaceuticals*. 2021; 14(11):1071. <https://doi.org/10.3390/ph14111071>
 26. Sandhiya, V., Ubaidulla, U. Enhancing cellular uptake and membrane permeability of gallic acid for breast cancer therapy via folate-tagged PEGylated iron oxide nanoparticles has theronastic agent. *Bull Natl Res Cent* 46, 234 (2022). <https://doi.org/10.1186/s42269-022-00909-7>
 27. Sulaiman, A. D. I., Adamu, M. B., Hassan, U., & Aliyu, S. M. (2021). Investigation into the Application of *Cissus Populnea* as Drilling Fluid Additive (Viscosifier) for Water Based Mud. *European Journal of Engineering and Technology Research*, 6(7), 33–37. <https://doi.org/10.24018/ejeng.2021.6.7.2611>
 28. Almkhtar, J. G. J., & Karam, F. F. (2020, November). Preparation characterization and application of Chitosan nanoparticles as drug carrier. In *Journal of Physics: Conference Series* (Vol. 1664, No. 1, p. 012071). IOP Publishing. <https://iopscience.iop.org/article/10.1088/1742-6596/1664/1/012071>
 29. Patil, P., & Killedar, S. (2021). Formulation and characterization of gallic acid and quercetin chitosan nanoparticles for sustained release in treating colorectal cancer. *Journal of Drug Delivery Science and Technology*, 63, 102523. <https://www.sciencedirect.com/science/article/abs/pii/S1773224721002033#:~:text=The%20present%20study%20was%20undertaken,tar geted%20delivery%20to%20colorectal%20cancer.>
 30. Lin, P. C., Lin, S., Wang, P. C., & Sridhar, R. (2014). Techniques for physicochemical characterization of nanomaterials. *Biotechnology advances*, 32(4), 711–726. <https://doi.org/10.1016/j.biotechadv.2013.11.006>
 31. Al-Thabaiti, S. A., Al-Nowaiser, F. M., Obaid, A. Y., Al-Youbi, A. O., & Khan, Z. (2008). Formation and characterization of surfactant stabilized silver nanoparticles: a kinetic study. *Colloids and Surfaces B: Biointerfaces*, 67(2), 230–237. <https://www.sciencedirect.com/science/article/abs/pii/S0927776508003263>
 32. Hassani, A., Azarian, M.M.S., Ibrahim, W.N. et al. Preparation, characterization and therapeutic properties of gum arabic-stabilized gallic acid nanoparticles. *Sci Rep* 10, 17808 (2020). <https://doi.org/10.1038/s41598-020-71175-8>
 33. Soltanzadeh M, Peighambari SH, Ghanbarzadeh B, Mohammadi M, Lorenzo JM. Chitosan Nanoparticles as a Promising Nanomaterial for Encapsulation of Pomegranate (*Punica granatum L.*) Peel Extract as a Natural Source of Antioxidants. *Nanomaterials*. 2021; 11(6):1439. <https://doi.org/10.3390/nano11061439>
 34. Cohen, D. J., Reynaldo, W. V., Borba, V. B., Theodoro, T. R., Petri, G., Cavalheiro, R. P., Mader, A. M., Han, S. W., Pinhal, M. A., & Glina, S. (2022). New in vivo model to assess macroscopic, histological, and molecular changes in Peyronie's disease. *Andrology*, 10(1), 154–165. <https://doi.org/10.1111/andr.13092>
 35. Lin, S., Qin, H. Z., Li, Z. Y., Zhu, H., Long, L., & Xu, L. B. (2022). Gallic acid suppresses the progression of triple-negative breast cancer HCC1806 cells via modulating PI3K/AKT/EGFR and MAPK signaling pathways. *Frontiers in Pharmacology*, 13. <https://www.frontiersin.org/articles/10.3389/fphar.2022.1049117>
 36. Skiba, J., Karpowicz, R., Szabo, I., Therrien, B., & Kowalski, K. (2015). Synthesis and anticancer activity studies of ferrocenyl-thymine-3, 6-dihydro-2H-thiopyranes—A new class of metallocene-nucleobase derivatives. *Journal of*

- Organometallic Chemistry, 794, 216-222. https://www.researchgate.net/publication/282307374_Synthesis_and_anticancer_activity_studies_of_ferrocenyl-thymine-36-dihydro-2H-thiopyranes_-_A_new_class_of_metallocene-nucleobase_derivatives
37. Liao, C., Xu, D., Liu, X., Fang, Y., Yi, J., Li, X., & Guo, B. (2018). Iridium (III) complex-loaded liposomes as a drug delivery system for lung cancer through mitochondrial dysfunction. *International journal of nanomedicine*, 13, 4417–4431. <https://doi.org/10.2147/IJN.S170035>
38. Bai, Y., Yang, Y., Cui, B., Lin, D., Wang, Z., & Ma, J. (2022). Temporal effect of melatonin posttreatment on anoxia/reoxygenation injury in H9c2 cells. *Cell biology international*, 46(4), 637–648. <https://doi.org/10.1002/cbin.11759>
39. Jingwen Zhang, Chengtian Zhao, Feifei Shi, Shaozhi Zhang, Sijie Wang, Xizeng Feng, Melatonin alleviates the deterioration of oocytes and hormonal disorders from mice subjected to glyphosate, *Molecular and Cellular Endocrinology*, Volume 520, 2021, 111073, ISSN 0303-7207. <https://doi.org/10.1016/j.mce.2020.111073>
40. Zhou, L. C., Liang, Y. F., Huang, Y., Yang, G. X., Zheng, L. L., Sun, J. M., Li, Y., Zhu, F. L., Qian, H. W., Wang, R., & Ma, L. (2021). Design, synthesis, and biological evaluation of diosgenin-indole derivatives as dual-functional agents for the treatment of Alzheimer's disease. *European journal of medicinal chemistry*, 219, 113426. <https://doi.org/10.1016/j.ejmech.2021.113426>
41. Zeng, M., Su, Y., Li, K., Jin, D., Li, Q., Li, Y., & Zhou, B. (2020). Gallic acid inhibits bladder cancer T24 cell progression through mitochondrial dysfunction and PI3K/Akt/NF- κ B signaling suppression. *Frontiers in Pharmacology*, 11, 1222. <https://www.frontiersin.org/articles/10.3389/fphar.2020.01222>
42. Dehghani, M. A., Shakiba Maram, N., Moghimipour, E., Khorsandi, L., Atefi Khah, M., & Mahdavinia, M. (2020). Protective effect of gallic acid and gallic acid-loaded Eudragit-RS 100 nanoparticles on cisplatin-induced mitochondrial dysfunction and inflammation in rat kidney. *Biochimica et biophysica acta. Molecular basis of disease*, 1866(12), 165911. <https://doi.org/10.1016/j.bbadis.2020.165911>
43. Hajipour, Hamed & Hamishehkar, Hamed & Rahmati, Mohammad & Shanehbandi, Dariush & Nazari Soltan Ahmad, Saeed & HASANI, Dr. AKBAR. (2018). Enhanced Anti-Cancer Capability of Ellagic Acid Using Solid Lipid Nanoparticles (SLNs). *International Journal of Cancer Management*. In Press. 10.5812/ijcm.9402. https://www.researchgate.net/publication/322970979_Enhanced_Anti-Cancer_Capability_of_Ellagic_Acid_Using_Solid_Lipid_Nanoparticles_SLNs
44. Patel, P., Raval, M., Manvar, A., Airao, V., Bhatt, V., & Shah, P. (2022). Lung cancer targeting efficiency of Silibinin loaded Poly Caprolactone /Pluronic F68 Inhalable nanoparticles: In vitro and In vivo study. *PloS one*, 17(5), e0267257. <https://doi.org/10.1371/journal.pone.0267257>